with liberal portions of ether, and dried in vacuo. A mass spectrometric analysis of gases above the reaction mixture showed the presence of CH_4.

Preparation of $[\eta^5\text{-}C_5H_5Cr(NO)_2L]PF_6$. A. By Reaction of $[\eta^5\text{-}C_5H_5Cr(NO)_2(CH_3CN)]PF_6$ with L (L = $C_6H_5NH_2$, $p\text{-}CH_3C_6H_4NH_2$, $p\text{-}ClC_6H_4NH_2$, C_5H_5N, $4\text{-}CH_3C_5H_4N$, CH_3NC). A solution of 0.2–1.0 g (0.55–2.7 mmol) of $[\eta^5\text{-}C_5H_5Cr(NO)_2(CH_3CN)]PF_6$ and a twofold to threefold excess of L in 25–75 mL of CH_3NO_2 was stirred at 25 °C for ca. 12 h. Solvent was removed from the reaction mixture, the residue was dissolved in a minimum amount of acetone, and the resulting solution was filtered and treated with 20–30 mL of $CHCl_3$. Storage at −78 °C for 4–12 h afforded $[\eta^5\text{-}C_5H_5Cr(NO)_2L]PF_6$ as green crystals which were collected on a frit, washed with $CHCl_3$, and dried in vacuo. The yield was 70–85%.

B. By Reaction of $\eta^5\text{-}C_5H_5Cr(NO)_2FPF_5$ with L (L = C_6H_5CN, $p\text{-}CH_3C_6H_4NH_2$, $C_6H_{11}NC$). Freshly prepared $\eta^5\text{-}C_5H_5Cr(NO)_2FPF_5$ was dissolved in CH_3NO_2, and the resulting solution was treated with excess L and stirred at 25 °C for 12 h. The rest of the procedure was identical with that of method A. The yield was 50–60%.

Preparation of $[\eta^5\text{-}C_5H_5Cr(NO)(L\text{–}L)]PF_6$ (L–L = phen, bpy). A solution of 0.30 g (0.82 mmol) of $[\eta^5\text{-}C_5H_5Cr(NO)_2(CH_3CN)]PF_6$ and a slight excess of L–L in 30 mL of CH_3NO_2 was kept at reflux for 4 h, during which time it changed from green to red-brown. Solvent was removed at 25 °C, the residue was dissolved in acetone, and the resulting solution was filtered and concentrated to ca. 5 mL. Treatment with 20 mL of $CHCl_3$, followed by slow evaporation of the solvent, afforded a red-brown precipitate which was collected on a frit, washed with $CHCl_3$, and dried in vacuo. The yield was 70–75%.

Preparation of $\eta^5\text{-}C_5H_5Cr(NO)_2[C(OCH_3)NCH_3]$. To a solution containing 0.20 g (0.55 mmol) of $[\eta^5\text{-}C_5H_5Cr(NO)_2(CH_3NC)]PF_6$ in 20 mL of CH_3OH was added 1.0 mL of 1.0 M (1.0 mmol) $NaOCH_3$ in CH_3OH. The mixture was stirred at 25 °C for 12 h, during which time it changed from green to gold. Solvent was removed, and the residue was cooled to −78 °C to prevent decomposition. It was then extracted with 10-mL portions of CH_2Cl_2 at 25 °C until the extracts became colorless. The extracts were combined, filtered, and freed of solvent to afford the title complex as a gold oil. Attempts at crystallization at ambient temperatures proved unsuccessful, owing to thermal instability of the complex.

Preparation of $\{\eta^5\text{-}C_5H_5Cr(NO)_2[C(OCH_3)NHCH_3]\}PF_6$. The filtered extracts containing $\eta^5\text{-}C_5H_5Cr(NO)_2[C(OCH_3)NCH_3]$ from the preceding preparation were treated with 0.10 mL (0.60 mmol) of $HPF_6\cdot(C_2H_5)_2O$ as the color changed from gold to green. The resulting solution was filtered and concentrated, and cyclohexane was added to induce precipitation of a green solid. The crude product was recrystallized from acetone–ether. The yield was 0.18 g (83% on the basis of $[\eta^5\text{-}C_5H_5Cr(NO)_2(CH_3NC)]PF_6$).

Preparation of $\{\eta^5\text{-}C_5H_5Cr(NO)_2[C(OC_2H_5)NHCH_3]\}PF_6$. This complex was prepared by a procedure strictly analogous to that for its OCH_3 analogue by using C_2H_5OH and $NaOC_2H_5$ in place of CH_3OH and $NaOCH_3$. The product was isolated as a green oil which could not be induced to crystallize.

Preparation of $\eta^5\text{-}C_5H_5Cr(NO)_2[C(O)NHCH_3]$. To a solution containing 0.20 g (0.55 mmol) of $[\eta^5\text{-}C_5H_5Cr(NO)_2(CH_3NC)]PF_6$ in 30 mL of CH_3CN was added 10 mL of aqueous 0.10 M (1.0 mmol) KOH. The mixture was stirred at 25 °C for 1 h, during which time it changed from green to red-brown. Solvent was removed, and the residue was cooled to −78 °C and extracted with CH_2Cl_2 at 25 °C until the extracts became colorless. The extracts were combined, filtered, and freed of solvent to yield a red-brown powder, which was spectroscopically characterized as the title complex. The product decomposed during attempts at crystallization at ambient temperatures.

Preparation of $[\eta^5\text{-}C_5H_5Cr(NO)_2(CO)]PF_6$. The product from the preceding reaction was dissolved in 15 mL of CH_3NO_2, and the resulting solution was treated with 0.20 mL (1.2 mmol) of $HPF_6\cdot(C_2H_5)_2O$ and stirred at 25 °C for 1 h as the color changed from red to green. Solvent was removed, and the residue was washed with 15 mL of H_2O and dried in vacuo. The crude product was recrystallized from acetone–ether to yield 0.04 g (20% on the basis of $[\eta^5\text{-}C_5H_5Cr(NO)_2(CH_3NC)]PF_6$) of $[\eta^5\text{-}C_5H_5Cr(NO)_2(CO)]PF_6$.

Acknowledgment. We are grateful to the National Science Foundation for support of this ressearch through Grant CHE-7911882.

Registry No. $[\eta^5\text{-}C_5H_5Cr(NO)_2(CH_3CN)]PF_6$, 74924-59-7; $\eta^5\text{-}C_5H_5Cr(NO)_2FPF_5$, 74924-60-0; $[\eta^5\text{-}C_5H_5Cr(NO)_2(C_6H_5NH_2)]PF_6$, 74924-62-2; $[\eta^5\text{-}C_5H_5Cr(NO)_2(p\text{-}CH_3C_6H_4NH_2)]PF_6$, 74924-64-4; $[\eta^5\text{-}C_5H_5Cr(NO)_2(C_5H_5N)]PF_6$, 74858-44-9; $[\eta^5\text{-}C_5H_5Cr(NO)_2(4\text{-}CH_3C_5H_4N)]PF_6$, 74924-66-6; $[\eta^5\text{-}C_5H_5Cr(NO)_2(p\text{-}ClC_6H_4NH_2)]PF_6$, 74924-68-8; $\eta^5\text{-}C_5H_5Cr(NO)_2[C(OCH_3)NCH_3]$, 74924-69-9; $[\eta^5\text{-}C_5H_5Cr(NO)_2[C(OCH_3)NHCH_3]]PF_6$, 74924-71-3; $[\eta^5\text{-}C_5H_5Cr(NO)_2[C(OC_2H_5)NHCH_3]]PF_6$, 74924-73-5; $\eta^5\text{-}C_5H_5Cr(NO)_2[C(O)NHCH_3]$, 74924-74-6; $[\eta^5\text{-}C_5H_5Cr(NO)_2(CO)]PF_6$, 69439-82-3; $[\eta^5\text{-}C_5H_5Cr(NO)_2(C_6H_{11}NC)]PF_6$, 74924-76-8; $[\eta^5\text{-}C_5H_5Cr(NO)(phen)]PF_6$, 74924-78-0; $[\eta^5\text{-}C_5H_5Cr(NO)(bpy)]PF_6$, 74924-80-4; $\eta^5\text{-}C_5H_5Cr(NO)_2Cl$, 12071-51-1; $\eta^5\text{-}C_5H_5Cr(NO)_2CH_3$, 53522-59-1; $[\eta^5\text{-}C_5H_5Cr(NO)_2(C_6H_5CN)]PF_6$, 74924-82-6; $[\eta^5\text{-}C_5H_5Cr(NO)_2(CH_3NC)]PF_6$, 74924-84-8.

Contribution from the Department of Applied Chemistry, Faculty of Engineering, Osaka University, Yamadakami, Suita-shi, Osaka-fu 565, Japan

Crystal Structure of Europium(II) Bromoborate

KEN-ICHI MACHIDA, GIN-YA ADACHI,* NORITAKE YASUOKA, NOBUTAMI KASAI, and JIRO SHIOKAWA

Received March 18, 1980

Needlelike single crystals of $Eu_2B_5O_9Br$ were grown from the molten sample containing a large excess of $EuBr_2$ as a flux. The crystal structure was determined from three-dimensional X-ray diffraction data (R = 0.047 for 1979 observed reflections, with anisotropic thermal parameters for Eu and Br atoms). The bromoborate $Eu_2B_5O_9Br$ is isostructural with the Ca analogue. The crystal belongs to the orthorhombic (pseudotetragonal) system, of space group *Pnn*2, with four formula units in a cell of dimensions a = 11.503 (3), b = 11.382 (3), and c = 6.484 (2) Å. The structure consists of a three-dimensional $(B_5O_9)_\infty$ network, in which B_5O_{12} groups of three BO_4 tetrahedra and two BO_3 triangles are linked together by sharing cornered oxygens. The Eu and Br atoms are located in tunnels of the $(B_5O_9)_\infty$ network extending along the c axis. Each Eu atom is surrounded by two Br atoms and seven O atoms with interatomic distances from 3.009 to 3.093 Å and from 2.526 to 3.061 Å, respectively.

Introduction

Divalent europium (Eu^{2+}) containing compounds have been investigated because of their magnetic[1-3] and spectroscopic[4] properties, which are closely related to the crystal structure, e.g., the distances between neighboring Eu^{2+} ions and the anion environment around the Eu^{2+} ion. The Eu^{2+}-activated alka-

(1) Matthias, B. T.; Bozorth, R. M.; Van Vleck, J. H. *Phys. Rev. Lett.* **1961**, *7*, 1960.
(2) Suits, J. C.; Lee, K. *J. Appl. Phys.* **1971**, *42*, 3258.
(3) Fan, G.; Burn, R. A. *J. Appl. Phys.* **1971**, *42*, 3458.
(4) (a) Blasse, G.; Bril, A. *Philips Tech. Rev.* **1970**, *31*, 304. (b) Blasse, G. *Struct. Bonding (Berlin)* **1976**, *26*, 43–79.

0020-1669/80/1319-3807$01.00/0

Table I. Crystal Data for $Eu_2B_5O_9Br$

fw 581.88	λ 0.710 69 Å
orthorhombic	μ(Mo Kα) = 19.264 mm^{-1}
space group: *Pnn*2 (34)	d_{measd} = 4.53 g cm^{-3}
a = 11.503 (3) Å	d_{calcd} = 4.55 g cm^{-3}
b = 11.382 (3)	Z = 4
c = 6.484 (2)	F(000) = 1032
V = 848.9 (4) Å^3	cryst size: 0.10 × 0.10 × 0.20 mm

line-earth (e.g., Ca, Sr, and Ba) compounds give the band or line emission based on the $4f^7$–$4f^65d$ or $4f^7$–$4f^7$ transition of Eu^{2+} ion. Particularly the halides give the blue emissions with high quantum efficiency and, at low temperature, the $4f^7$–$4f^7$ line spectra are also observed on most of them.[5] Recently we have reported that the quantum efficiencies of Eu^{2+}-activated phosphors in a system SrO–B_2O_3 greatly depend on the structural frameworks of borate units.[6]

In a ternary system MO–MX_2–B_2O_3 (M = Ca, Sr, Ba, Eu, Pb; X = Cl, Br), $M_2B_5O_9X$ type compounds have been obtained in the attempts to prepare their boracite ($Mg_3B_7O_{13}Cl$) analogues.[7] No boracite type compound has been obtained in this system. The europium(II) haloborates, $Eu_2B_5O_9Cl$ and $Eu_2B_5O_9Br$, are paramagnetic and give the blue emissions.[7c] The compounds that diluted the Eu^{2+} ions in $Eu_2B_5O_9X$ matrix with alkaline-earth cations have been found to be efficient photoluminescent materials.[7a] This paper reports the crystal structure of $Eu_2B_5O_9Br$, and its luminescence and magnetic properties are discussed on the basis of the X-ray structural analysis.

Experimental Section

Sample Preparation. The europium(II) haloborates are obtained from some raw materials, EuB_2O_4, EuX_2, and B_2O_3.[7c] The preparation method of EuB_2O_4 is described elsewhere,[6b] and EuX_2 can be easily prepared by heating $EuX_3 \cdot nH_2O$ together with a large excess of NH_4X at 650–700 °C for several hours in a reducing atmosphere. Consequently, the single crystals of $Eu_2B_5O_9Br$ were prepared as follows: the appropriate amounts of EuB_2O_4 and B_2O_3 and a large excess of $EuBr_2$ were fully mixed. The mixture was heated on a molybdenum boat above the congruent melting point of $Eu_2B_5O_9Br$ (about 1100 °C) for 2 h in an inert gas, e.g., He, and then the molten sample was allowed to cool at a rate of 3–5 °C/h to 950 °C. The unreactive $EuBr_2$ served as a flux and was removed from the resulting materials by washing with water. The needlelike light yellow crystals (~2 mm long) were obtained.

The Eu^{2+}-activated strontium bromoborate $Sr_2B_5O_9Br$:Eu^{2+} was prepared by heating the stoichiometric mixture of $SrBr_2$, H_3BO_3, and $SrCO_3$:Eu^{3+}, coprecipitated from a dilute HCl solution of $Sr(NO_3)_2$ at 950 °C for 2 h in a H_2 stream. The bromide, $SrBr_2$:Eu^{2+}, was formed when the precipitate $SrBr_2$:Eu^{3+} from an aqueous solution was heated at 650 °C for 2 h in a H_2 stream. The resulting materials were checked by the powder X-ray analysis.

Optical and Magnetic Susceptibility Measurements. The ultraviolet luminescence spectra of powder samples were measured according to the technique described in previous papers.[6] Magnetic susceptibility measurements were carried out with a Shimadzu MB-11 instrument over a temperature range of 80–300 K.

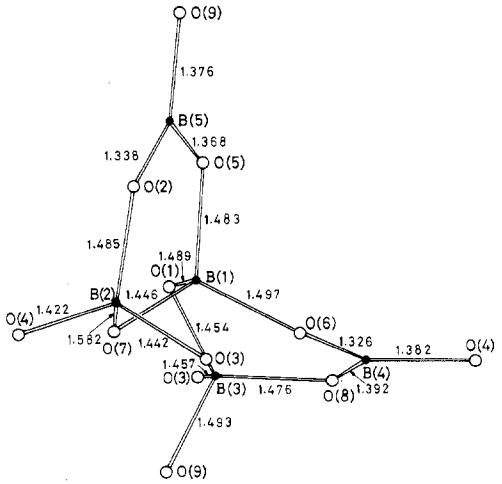

Figure 1. Projection of the B_5O_{12} group viewed along the c axis. The bond lengths in Å are given.

Crystallographic Measurements. Preliminary Weissenberg photographs (Cu Kα) showed that the crystals belong to the orthorhombic (pseudotetragonal) system, and the observed systematic absences of reflections ($k + l = 2n + 1$ for $0kl$ and $h + l = 2n + 1$ for $h0l$) showed the corresponding space group to be either *Pnn*2 or *Pnnm*. The accurate cell parameters (Table I) were determined by a least-squares treatment of the X-ray powder pattern (Cu $K\alpha_1$) calibrated with high-purity silicon as an internal standard. The intensity data were measured on a Rigaku automated four-circle diffractometer with graphite-monochromatized Mo Kα radiation. The ω–2θ scan method was employed with a scanning rate of 4°/min. The stationary-crystal and stationary-counter background counts were measured at the beginning and end of the ω–2θ scan for one-fourth of the scan time taken on each reflection. All possible reflections were collected out to the 2θ value of 70°. Three standard reflections were monitored every 60 reflections, and no apparent decay in intensity was detected. The 2017 unique reflections were obtained, among which 1979 reflections with $F_o > 3\sigma_{F_o}$ were considered as observed. The usual Lorentz and polarization corrections were applied, but the absorption and anomalous dispersion effects for heavy atoms were not considered.

Structure Determination and Refinement. The structure was solved by the conventional heavy-atom method and was refined by the block-diagonal least-squares method (HBLS-V program[8]), the function minimized being $\sum w(|F_o| - |F_c|)^2$. From a three-dimensional Patterson function, the space group of $Eu_2B_5O_9Br$ was found to be the noncentrosymmetric *Pnn*2 and the coordinates of Eu and Br atoms were determined. All major peaks on the Patterson map could be explained by locating the Eu atoms at the general positions (4c site) and Br atoms at the special positions (2a and 2b sites): Eu(1) at 0.25, 0.05, 0.00; Eu(2) at 0.03, 0.25, 0.66; Br(1) at 0.00, 0.00, 0.88; Br(2) at 0.00, 0.50, 0.66. The structure factors based on these coordinates, with the assumption of an isotropic thermal factor of 0.5 Å^2 for each atom, gave $R = \sum||F_o| - |F_c||/\sum|F_o| = 0.40$, which reduced to 0.13 after three cycles of refinement. The remaining atoms, O and B, were located on the successive Fourier maps. Three cycles of isotropic refinement gave a conventional R value of 0.060. Further refinements with anisotropic temperature factors applied for Eu and Br atoms reduced R and R_w to 0.047 and 0.053, respectively, where $R_w = [\sum w(|F_o| - |F_c|)^2/\sum w(F_o)^2]^{1/2}$. The weighting scheme $w = (F_m/F_o)^2$ for $F_o > F_m$ (=40.0) and $w = 1.0$ for $F_o \leq F_m$ (=40.0) was employed in order to determine the coordinates of light atoms more accurately. The atomic scattering factors used in all the calculations were taken from ref 9. The final positional and thermal parameters along with their estimated standard deviations are listed in Table II.

(5) (a) Hewes, R. A.; Hoffman, M. V. *J. Lumin.* **1971**, *3*, 261. (b) Meehan, J. P.; Wilson, E. J. *J. Cryst. Growth* **1972**, *15*, 141. (c) Hoffman, M. V. *J. Electrochem. Soc.* **1972**, *119*, 905. (d) Altshuler, N. S.; Livanova, L. D.; Stolov, A. L. *Opt. Spectrosc. (Engl. Transl.)* **1974**, *36*, 72. (e) Sommerdijk, J. L.; Verstegen, J. M. P. J.; Bril, A. *J. Lumin.* **1974**, *8*, 502. (f) Brixner, L. H.; Bierlein, J. D. *Mater. Res. Bull.* **1974**, *9*, 99. (g) Tanguy, B.; Merle, P.; Pezat, M.; Fouassier, C. *Ibid.* **1974**, *9*, 831. (h) Stevels, A. L. N.; Pingault, F. *Philips Res. Rep.* **1975**, *30*, 277. (i) Brixner, L. H.; Ferretti, A. *J. Solid State Chem.* **1976**, *18*, 111. (j) Valon, P.; Cousseins, J. C.; Vedrine, A.; Gacon, J. C.; Boulon, G.; Fong, F. K. *Mater. Res. Bull.* **1976**, *11*, 43. (k) Latourrette, B.; Grannec, J.; Fouassier, C.; Hagenmuller, P. *Ibid.* **1976**, *11*, 135. (l) Brixner, L. H. *Ibid.* **1976**, *11*, 269.

(6) (a) Machida, K.; Adachi, G.; Shiokawa, J. *J. Lumin.* **1979**, *21*, 101. (b) Machida, K.; Adachi, G.; Shiokawa, J.; Shimada, M.; Koizumi, M. *Inorg. Chem.* **1980**, *19*, 983.

(7) (a) Peters, T. E.; Baglio, J. *J. Inorg. Nucl. Chem.* **1970**, *32*, 1089. (b) Fouassier, C.; Levasseur, A.; Hagenmuller, P. *J. Solid State Chem.* **1971**, *3*, 206. (c) Machida, K.; Ishino, T.; Adachi, G.; Shiokawa, J. *Mater. Res. Bull.* **1979**, *14*, 1529.

(8) Ashida, T. "The Universal Crystallographic Computing System—Osaka"; The Computation Center, Osaka University: Osaka, Japan, 1979; pp 53–59.

(9) "International Tables for X-ray Crystallography"; Kynoch Press: Birmingham, England, 1974; Vol. IV, pp 99–101.

Table II. Positional and Thermal Parameters and Their Estimated Standard Deviations for $Eu_2B_5O_9Br$

atom	x	y	z	U_{11}[a]	U_{22}	U_{33}	U_{12}	U_{13}	U_{23}
Eu(1)	0.2547 (6)	0.0501 (6)	0.0000 (0)	76 (2)	77 (2)	84 (2)	12 (2)	−12 (2)	−10 (2)
Eu(2)	0.0307 (6)	0.2374 (6)	0.6572 (10)	62 (2)	92 (2)	77 (2)	−4 (2)	−16 (2)	1 (3)
Br(1)	0.0000 (0)	0.0000 (0)	0.8769 (27)	95 (7)	107 (7)	244 (10)	−19 (6)	0 (0)	0 (0)
Br(2)	0.0000 (0)	0.5000 (0)	0.6370 (32)	75 (6)	111 (7)	357 (13)	2 (5)	0 (0)	0 (0)

atom	x	y	z	B, Å^2	atom	x	y	z	B, Å^2
O(1)	0.246 (9)	0.318 (9)	0.581 (9)	0.40 (11)	O(8)	0.423 (9)	0.212 (9)	0.500 (11)	0.66 (11)
O(2)	0.209 (9)	0.427 (9)	0.182 (10)	0.59 (12)	O(9)	0.239 (9)	0.115 (9)	0.571 (10)	0.62 (12)
O(3)	0.279 (9)	0.227 (9)	0.248 (10)	0.59 (12)	B(1)	0.275 (12)	0.326 (12)	0.805 (13)	0.17 (13)
O(4)	0.078 (9)	0.267 (9)	0.254 (10)	0.69 (12)	B(2)	0.187 (12)	0.299 (12)	0.167 (17)	0.54 (14)
O(5)	0.283 (10)	0.454 (9)	0.844 (11)	0.76 (12)	B(3)	0.295 (12)	0.218 (12)	0.471 (13)	0.39 (15)
O(6)	0.388 (10)	0.266 (10)	0.847 (10)	0.76 (12)	B(4)	0.462 (14)	0.236 (15)	0.699 (14)	0.72 (18)
O(7)	0.185 (9)	0.271 (8)	0.928 (9)	0.35 (10)	B(5)	0.248 (12)	0.497 (12)	0.031 (12)	0.29 (14)

[a] The form of the anisotropic thermal parameter ($\times 10^4$) is $\exp[-2\pi^2(U_{11}h^2a^{*2} + U_{22}k^2b^{*2} + U_{33}l^2c^{*2} + 2U_{12}hka^*b^* + 2U_{13}hla^*c^* + 2U_{23}klb^*c^*)]$.

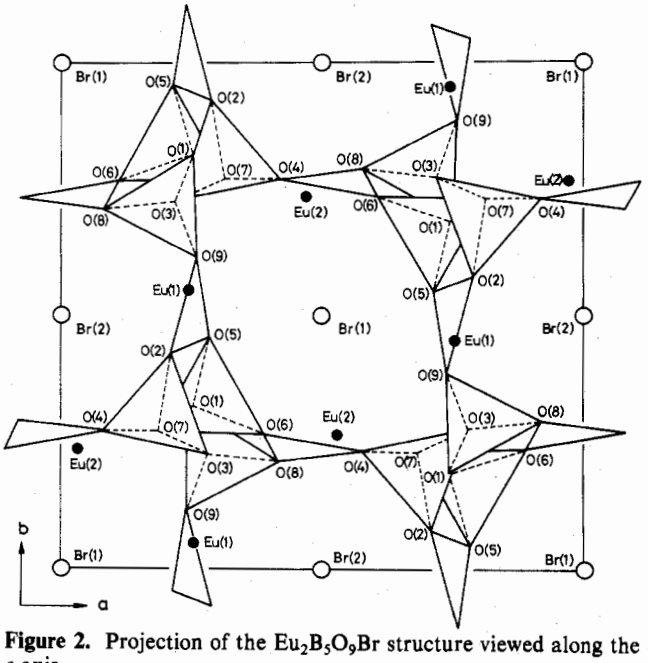

Figure 2. Projection of the $Eu_2B_5O_9Br$ structure viewed along the c axis.

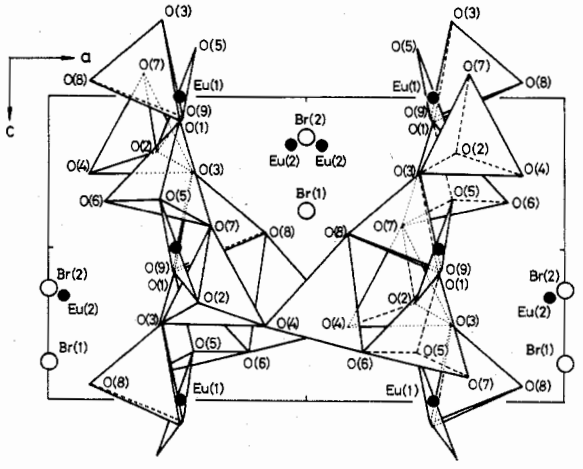

Figure 3. Projection of the $Eu_2B_5O_9Br$ structure viewed along the b axis.

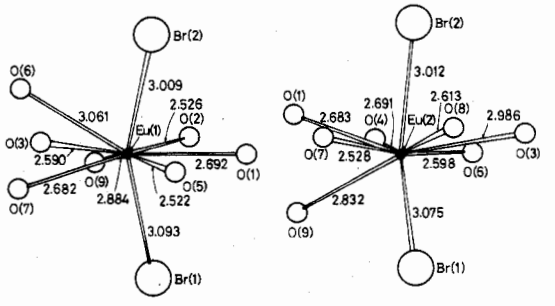

Figure 4. Anion environments around Eu(1) and Eu(2) atoms. Numerical values represent the nearest-neighboring Eu–Br and Eu–O distances in Å.

Results and Discussion

The final atomic parameters of $Eu_2B_5O_9Br$ (Table II) are almost equal to those of $Ca_2B_5O_9Br$ reported by Lloyd et al.,[10] and hence two haloborates are isostructural. The interatomic distances and angles along with their estimated standard deviations are presented in Table III. There are two types of B atoms: three of them [B(1), B(2), and B(3)] are tetrahedrally coordinated with mean B–O distances from 1.446 to 1.483 Å and two [B(4) and B(5)] are triangularly coordinated with mean B–O distances 1.367 and 1.361 Å. The mean O–B–O angles are about 109° for tetrahedra and 120° for triangles, respectively. Three tetrahedra and two triangles form a B_5O_{12} group (Figure 1) by sharing O atoms. In this group, O(1) and O(7) atoms are shared with other BO_4 tetrahedra and O(2), O(5), O(6), and O(8) atoms are shared with BO_4 tetrahedra and BO_3 triangles. These groups are linked together to form a three-dimensional $(B_5O_9)_\infty$ network by sharing O(3), O(4), and O(9) atoms with one another. The projections of the $Eu_2B_5O_9Br$ structure viewed along the c and b axes are shown in Figures 2 and 3, respectively. The structure consists of chains of corner-sharing BO_4 tetrahedra which extend along the c axis, and they are linked in the a- and b-axis directions by B(4) and B(5) atoms which occupy the centers of triangles of O atoms.

The Eu and Br atoms are located alternately with each other in tunnels of the $(B_5O_9)_\infty$ network, and each Eu atom is considerably isolated from neighboring Eu atoms by the borate units of the $(B_5O_9)_\infty$ network in the a- and b-axis directions and Br atoms in the c-axis direction. The anion environments around Eu(1) and Eu(2) atoms are shown in Figure 4. The Eu atoms are surrounded by two Br atoms and seven O atoms to form a EuO_7Br_2 polyhedron with Eu–Br distances from 3.009 to 3.093 Å and Eu–O distances from 2.526 to 3.061 Å, respectively.

The luminescence properties of some Eu^{2+} phosphors are summarized in Table IV. The bromoborate $Eu_2B_5O_9Br$ emits the $4f^7$–$4f^65d$ band spectrum with half-width of 30 nm peaking at 435 nm, and this peak position is near to that (422 nm) of $EuBr_2$ as one of raw materials but considerably different from

(10) Lloyd, M. D. J.; Levasseur, A.; Fouassier, C. *J. Solid State Chem.* **1973**, *6*, 179.

Table III. Interatomic Distances (Å) and Angles (Deg) for $Eu_2B_5O_9Br$

(a) Distances and Angles of the $(B_5O_9)_\infty$ Network

	B(1)-Tetrahedron		
B(1)-O(1)	1.489 (16)	O(1)-B(1)-O(5)	103.9 (9)
B(1)-O(5)	1.483 (16)	O(1)-B(1)-O(6)	110.2 (10)
B(1)-O(6)	1.497 (16)	O(1)-B(1)-O(7)	110.5 (10)
B(1)-O(7)	1.446 (15)	O(5)-B(1)-O(6)	111.3 (10)
average	1.479	O(5)-B(1)-O(7)	112.1 (10)
		O(6)-B(1)-O(7)	108.8 (10)
		average	109.5
	B(2)-Tetrahedron		
B(2)-O(2)	1.485 (20)	O(2)-B(2)-O(3)	114.6 (12)
B(2)-O(3)	1.443 (19)	O(2)-B(2)-O(4)	111.6 (12)
B(2)-O(4)	1.422 (20)	O(2)-B(2)-O(7)	105.2 (13)
B(2)-O(7)	1.582 (19)	O(3)-B(2)-O(4)	111.1 (13)
average	1.483	O(3)-B(2)-O(7)	104.5 (13)
		O(4)-B(2)-O(7)	108.9 (13)
		average	109.3
	B(3)-Tetrahedron		
B(3)-O(1)	1.454 (16)	O(1)-B(3)-O(3)	112.8 (10)
B(3)-O(3)	1.457 (16)	O(1)-B(3)-O(8)	111.4 (10)
B(3)-O(8)	1.476 (17)	O(1)-B(3)-O(9)	103.3 (10)
B(3)-O(9)	1.493 (17)	O(3)-B(3)-O(8)	104.8 (10)
average	1.470	O(3)-B(3)-O(9)	115.2 (10)
		O(8)-B(3)-O(9)	109.6 (10)
		average	109.5
	B(4)-Triangle		
B(4)-O(4)	1.382 (18)	O(4)-B(4)-O(6)	116.1 (13)
B(4)-O(6)	1.326 (18)	O(4)-B(4)-O(8)	123.1 (13)
B(4)-O(8)	1.392 (18)	O(6)-B(4)-O(8)	120.9 (13)
average	1.367	average	120.0
	B(5)-Triangle		
B(5)-O(2)	1.338 (16)	O(2)-B(5)-O(5)	122.4 (10)
B(5)-O(5)	1.368 (16)	O(2)-B(5)-O(9)	118.8 (10)
B(5)-O(9)	1.376 (16)	O(5)-B(5)-O(9)	119.0 (10)
average	1.361	average	120.1

(b) Eu-Eu Distances[a]

	Nearest Neighbors		
Eu(1)-Eu(2)	4.014 (1)	Eu(1)-Eu(2''')	4.122 (1)
Eu(1)-Eu(2')	5.142 (1)	average	4.432
Eu(1)-Eu(2'')	4.448 (1)		
	Next-Nearest Neighbors		
Eu(1)-Eu(1')	5.750 (1)	Eu(1)-Eu(2)	5.415 (1)
	5.976 (1)	Eu(1)-Eu(2')	6.296 (1)
Eu(2)-Eu(2')	5.442 (1)		
	6.029 (1)		

(c) Eu-Br and Eu-O Distances

	Eu(1) Polyhedron		
Eu(1)-Br(1)	3.093 (3)	Eu(1)-O(3)	2.590 (10)
Eu(1)-Br(2)	3.009 (3)	Eu(1)-O(5)	2.522 (11)
average	3.051	Eu(1)-O(6)	3.061 (11)
Eu(1)-O(1)	2.692 (9)	Eu(1)-O(7)	2.682 (9)
Eu(1)-O(2)	2.526 (10)	Eu(1)-O(9)	2.884 (10)
		average	2.708
	Eu(2) Polyhedron		
Eu(2)-Br(1)	3.075 (3)	Eu(2)-O(4)	2.691 (10)
Eu(2)-Br(2)	3.012 (3)	Eu(2)-O(6)	2.598 (11)
average	3.044	Eu(2)-O(7)	2.528 (9)
Eu(2)-O(1)	2.683 (9)	Eu(2)-O(8)	2.613 (11)
Eu(2)-O(3)	2.986 (10)	Eu(2)-O(9)	2.832 (10)
		average	2.704

[a] Symmetry transformations: Eu(1'), $(\bar{x}, \bar{y}, z)$; Eu(2'), $(\bar{x}, \bar{y}, z)$; Eu(2''), $(^1/_2 - x, ^1/_2 + y, ^1/_2 + z)$; Eu(2'''), $(^1/_2 + x, ^1/_2 - y, ^1/_2 + z)$.

that (370 nm) of another raw material, α-EuB_2O_4 (atmospheric phase). This suggests that the degrees for crystal field splitting and Stokes shifts of $4f^7$–$4f^65d$ levels in these compounds are different from one another. The Eu^{2+} ion in α-EuB_2O_4 is surrounded by eight oxygens to form a EuO_8 polyhedron with Eu–O distances 2.519–2.738 Å.[11] The

Table IV. Luminescence Properties for Some Eu^{2+}-Containing Compounds

compd	λ_{max},[a] nm	$\lambda/2$,[b] nm	QE,[c] % 254-nm excitation	QE,[c] % optimum excitation
$Eu_2B_5O_9Br$	435	30	5	7 (350)
$(Sr_{0.93}Eu_{0.07})_2B_5O_9Br$	430	30	46	62 (350)
$EuBr_2$	422	27	12	21 (370)
$Sr_{0.99}Eu_{0.01}Br_2$	411	22	20	42 (370)
α-EuB_2O_4	370	20	negligible	
α-$Sr_{0.97}Eu_{0.03}B_2O_4$	367	20	2	2 (250)

[a] λ_{max} = position of the maximum of emission band. [b] $\lambda/2$ = half-width of the emission band. [c] QE = quantum efficiency at 300 K. The values in parentheses represent the wavelengths for optimum excitation.

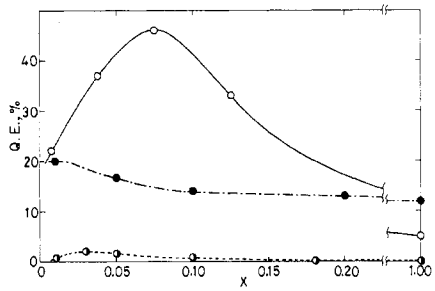

Figure 5. Quantum efficiency vs. Eu^{2+} content, x, for the emission bands under 254-nm excitation of $(Sr_{1-x}Eu_x)_2B_5O_9Br$ (○), $Sr_{1-x}Eu_xBr_2$ (●), and $Sr_{1-x}Eu_xB_2O_4$ (◑).

symmetry of the EuO_8 polyhedron differs from that of the EuO_7Br_2 polyhedron (Figure 4) in $Eu_2B_5O_9Br$ because of the large Br^- ions: the symmetry of the EuO_7Br_2 polyhedron is low. This difference must reflect the degrees of crystal field splitting and Stokes shift.

It is seen from Table IV that $Sr_2B_5O_9Br$:Eu^{2+} and $SrBr_2$:Eu^{2+} give the blue emissions with high quantum efficiency (about 60% under 350-nm excitation for the former compound and about 40% under 370-nm excitation for the latter compound) and are efficient phosphors. Particularly, the quantum efficiencies of $Eu_2B_5O_9Br$ and $EuBr_2$ are noticed to be considerably high compared with that of α-EuB_2O_4, although the concentration quenching effects in these materials are expected to be large.

In Figure 5, we show the concentration quenching curves for $(Sr_{1-x}Eu_x)_2B_5O_9Br$, $Sr_{1-x}Eu_xBr_2$, and $Sr_{1-x}Eu_xB_2O_4$. The curve of $(Sr_{1-x}Eu_x)_2B_5O_9Br$ or $Sr_{1-x}Eu_xB_2O_4$ has a maximum at about 7 or 3 atom %. For $Sr_{1-x}Eu_xBr_2$, however, the quantum efficiency does not apparently depend on the value of x: the slope of this curve is much flatter than those of other curves.

One of the quenching effects on Eu^{2+}-activated phosphors is a nonradiative process via Coulomb (dipole–dipole) interactions and exchange interactions between neighboring Eu^{2+} ions.[4a] Blasse has defined a critical distance R_c, which represents the distance between two luminescent centers, S (sensitizer) and A (activator), at which the probability of transfer from S to A is equal to the probability of radiative emission of S.[12] The R_c distances for most of Eu^{2+} phosphors have been estimated at 20–25 Å for the Coulomb interactions and 4–5 Å for exchange interactions, respectively. For the Eu^{2+} phosphors the Coulomb interactions are effective for one

(11) Machida, K.; Adachi, G.; Shiokawa, J. *Acta Crystallogr., Sect. B* **1979**, *B35*, 149.
(12) Blasse, G. *Philips Res. Rep.* **1969**, *24*, 131.

Table V. Magnetic and Structural Properties for Some Eu(II) Compounds

compd	magnetism	μ_{eff},[a] μ_B	T_N, K	Θ_c,[b] K	CN[c]	mean Eu–Eu dist,[d] Å: nn	mean Eu–Eu dist,[d] Å: nnn
$Eu_2B_5O_9Br$	paramagnetic	7.73		≃0	Eu(1) 9, Eu(2) 9	4.432 (×4)	5.589 (×4) 5.796 (×4)
$EuBr_2$[e]	paramagnetic	7.87		0	Eu(1) 7, Eu(2) 8	4.98 (×9) 4.86 (×8)	6.19 (×5) 5.99 (×4)
α-EuB_2O_4[f]	antiferromagnetic	7.88	≃3	−5	8	4.080 (×6)	6.632 (×10)

[a] μ_{eff} = magnetic moment per Eu^{2+} ion. The theoretical value is 7.94 μ_B. [b] Θ_c = paramagnetic Curie temperature. The measured temperature range is 80–300 K. [c] CN = Eu coordination number to anions. [d] nn and nnn represent the nearest Eu neighbors and next-nearest Eu neighbors, respectively. [e] The bromide $EuBr_2$ is isostructural with $SrBr_2$.[15] [f] References 6b and 11.

of the quenching effects, but the luminescence properties of high-concentration Eu^{2+}-containing samples, e.g., Eu(II) compounds, should be understood on the basis of the Coulomb and exchange interactions.

The magnetic and structural properties of $Eu_2B_5O_9Br$, $EuBr_2$, and α-EuB_2O_4 are summarized in Table V. The two compounds $Eu_2B_5O_9Br$ and $EuBr_2$ are paramagnetic while α-EuB_2O_4 is antiferromagnetic below about 3 K.[6b] The magnetisms of Eu(II) compounds are interpreted from the magnitude of magnetic exchange and superexchange interactions via the overlap of 4f and 5d orbitals between nearest- and next-nearest-neighboring Eu^{2+} ions, which is a strong function of the interatomic Eu^{2+} spacing and Eu^{2+}–O^{2-}–Eu^{2+} angle.[13] The Eu atoms in $Eu_2B_5O_9Br$ have four nearest Eu neighbors with the mean Eu–Eu distance 4.432 Å and four next-nearest Eu neighbors with the mean Eu–Eu distance 5.589 Å for the Eu(1) atom or 5.796 Å for the Eu(2) atom. These Eu–Eu distances are very long compared with those of other Eu(II) compounds with unique magnetic properties,[14] e.g., EuO (3.63 Å for six nearest Eu neighbors and 5.14 Å for twelve next-nearest Eu neighbors), and are insufficient for the above-mentioned magnetic interactions. The bromide $EuBr_2$ is isostructural with $SrBr_2$, and the Eu atoms have nine or eight nearest Eu neighbors with the mean Eu–Eu distance 4.98 or 4.86 Å and five or four next-nearest Eu neighbors with the Eu–Eu distance 6.19 or 5.99 Å for the Eu(1) or Eu(2) atom.[15] These distances are also entirely insufficient for the magnetic interactions. For α-EuB_2O_4, however, the 99 and 100° Eu $^{2+}$–O^{2-}–Eu^{2+} superexchange pairs are effective and antiferromagnetically contribute to the overall magnetism.[6b] The difference in the magnetisms of these compounds must reflect on their luminescence properties. For $Eu_2B_5O_9Br$ and $EuBr_2$, the quenching effect of exchange interactions is expected to be very small, but the quenching effect in α-EuB_2O_4 is not. This agrees with the fact that the former compounds give emissions with very high quantum efficiency compared with that of the latter compound.

The observation that the concentration quenching curve of $Sr_{1-x}Eu_xBr_2$ has a flatter slope than those of $(Sr_{1-x}Eu_x)_2B_5O_9Br$ and $Sr_{1-x}Eu_xB_2O_4$ (Figure 5) suggests that the quenching effect of Coulomb interactions in bromides is also small and the Br^- ions around Eu^{2+} ions may be excellent in the property of electrostatic shield. For $(Sr_{1-x}Eu_x)_2B_5O_9Br$ and $Sr_{1-x}Eu_xB_2O_4$, the concentration quenching curves have the maximum, respectively. This suggests that the quenching effect of Coulomb interactions is effective in these compounds. The Eu^{2+} ions in $Eu_2B_5O_9Br$ are located alternately with Br^- ions in tunnels of the $(B_5O_9)_\infty$ network, and each Eu^{2+} ion is isolated from the neighboring Eu^{2+} ions by the borate units of the $(B_5O_9)_\infty$ network in the *a*- and *b*-axis directions and Br^- ions in the *c*-axis direction. The energy transfers via Coulomb interactions are expected to take place mainly in the *a*- and *b*-axis directions, in which no Br^- ion is located. The fact that the emission of $Sr_{1-x}Eu_xB_2O_4$ is very weak is due to the cluster formation of Eu^{2+} ions in the matrix.[6b]

Conclusion

The structural framework of $Eu_2B_5O_9Br$ is the $(B_5O_9)_\infty$ network, in which the B_5O_{12} groups of three BO_4 tetrahedra and two BO_3 triangles are three-dimensionally linked together. The Eu^{2+} ion is surrounded by two Br^- ions and seven O^{2-} ions to form the EuO_7Br_2 polyhedron, and the Eu^{2+} ions in the polyhedra give the emission with half-width of 30 nm peaking at 435 nm. Each Eu^{2+} ion in $Sr_2B_5O_9Br$:Eu^{2+} is located alternately with Br^- ions in tunnels of the $(B_5O_9)_\infty$ network and is considerably isolated from neighboring Eu^{2+} ions by the borate units and Br^- ions. These anions are expected to reduce the quenching effects of Coulomb and exchange interactions, and hence $Sr_2B_5O_9Br$:Eu^{2+} gives the emission with high quantum efficiency.

Acknowledgment. The authors wish to thank Mr. K. Sakaguchi for the measurements on the four-circle X-ray diffractometer and Dr. N. Tanaka and Mr. K. Miki for their helpful suggestions throughout this study. The computations were carried out on an ACOS series 77 NEAC System 700 computer at the Crystallographic Research Center of the Institute for Protein Research, Osaka University.

Registry No. $Eu_2B_5O_9Br$, 12536-68-4; $Sr_2B_5O_9Br$, 12505-87-2; $EuBr_2$, 13780-48-8; $SrBr_2$, 10476-81-0; α-EuB_2O_4, 38313-81-4; α-SrB_2O_4, 13703-84-9.

Supplementary Material Available: A listing of structure factors (5 pages). Ordering information is given on any current masthead page.

(13) (a) McGuire, T. R.; Shafer, M. W. *J. Appl. Phys.* **1964**, *35*, 984. (b) Kasuya, T. *IBM J. Res. Dev.* **1970**, *14*, 214.
(14) Greedan, J. E.; McCarthy, G. J. *Mater. Res. Bull.* **1972**, *7*, 531.
(15) Smeggil, J. G.; Eick, H. A. *Inorg. Chem.* **1971**, *10*, 1458.